

M³D-Stereo: A Multiple-Medium and Multiple-Degradation Dataset for Stereo Image Restoration

Deqing Yang
Shenzhen University
Shenzhen, China
2410095078@mails.szu.edu.cn

Yingying Liu
Shenzhen University
Shenzhen, China
liuyying@szu.edu.cn

Qicong Wang
Shenzhen University
Shenzhen, China
2310295091@email.szu.edu.cn

Zhi Zeng
Chongqing Normal University
Chongqing, China
zh406@cqnu.edu.cn

Dajiang Lu*
Shenzhen University
Shenzhen, China
ludajiang@szu.edu.cn

Yibin Tian†
Shenzhen University
Shenzhen, China
ybtian@szu.edu.cn

Abstract

Image restoration under adverse conditions, such as underwater, haze or fog, and low-light environments, remains a highly challenging problem due to complex physical degradations and severe information loss. Existing datasets are predominantly limited to a single degradation type or heavily rely on synthetic data without stereo consistency, inherently restricting their applicability in real-world scenarios. To address this, we introduce M³D-Stereo, a stereo dataset with 7904 high-resolution image pairs for image restoration research acquired in multiple media with multiple controlled degradation levels. It encompasses four degradation scenarios: underwater scatter, haze/fog, underwater low-light, and haze low-light. Each scenario forms a subset, and is divided into six levels of progressive degradation, allowing fine-grained evaluations of restoration methods with increasing severity of degradation. Collected via a laboratory setup, the dataset provides aligned stereo image pairs along with their pixel-wise consistent clear ground truths. Two restoration tasks, single-level and mixed-level degradation, were performed to verify its validity. M³D-Stereo establishes a better controlled and more realistic benchmark to evaluate image restoration and stereo matching methods in complex degradation environments. It is made public under LGPLv3 license.

Keywords

Image restoration, stereo vision, underwater, haze/fog, low light, image quality

1 Introduction

Image restoration in degraded environments, including underwater [16, 40], haze/fog [12, 25], and low-light conditions [10, 37], has become increasingly important for applications such as autonomous navigation, marine exploration, and virtual reality. Although monocular restoration has been widely studied for these degradation scenarios [12, 37], it ignores the geometric consistency available in stereo imaging and often fails to recover fine details under severe degradation. Stereo restoration offers a promising alternative that uses cross-view fusion and geometric constraints to compensate for information loss.

However, the development of stereo restoration is challenged by the lack of suitable benchmark datasets. Existing stereo datasets, such as KITTI [9], mainly target disparity estimation and lack clear pixel-aligned images for photometric evaluation. In contrast, existing restoration datasets, such as UIEB [18] and O-HAZE [3], are largely monocular and therefore unsuitable for studying stereo-consistent restoration. In addition, synthetic data cannot faithfully reproduce the complex physical effects of real degraded environments, such as multiple scatter and photon noise [1]. As a result, current datasets typically suffer from one or more limitations: (1) focusing on only a single degradation scenario; (2) relying predominantly on synthetic data; and (3) lacking fine-grained control over degradation severity.

To address these limitations, we introduce M³D-Stereo (Multiple-Medium, Multiple-Degradation Stereo), a dataset for stereo image restoration. It covers four realistic degradation scenarios: underwater scatter (UWST), haze/fog scatter (HZST), underwater low-light (UWLL), and coupled haze and low-light (HZLL). Each scenario is divided into six progressive degradation levels (D1–D6), allowing controlled evaluation under increasing severity of degradation.

The dataset was built using a custom acquisition platform with two calibrated stereo camera systems and a turbidity-controllable imaging chamber. To enrich structural and semantic diversity, we constructed scenes using corals, rocks, aquatic plants, miniature vehicles, and figurines [27, 33]. For every pair of degraded stereo images, a clear reference was captured without degradation under the same scene and camera configuration [18]. This ensures pixel-wise alignment for photometric evaluation and also enables accurate disparity ground truths (GTs) to be derived from clear stereo pairs, providing useful geometric supervision for future stereo restoration and stereo matching studies [15, 28].

Compared with existing datasets, M³D-Stereo offers several distinct advantages: (1) It provides aligned stereo image pairs under realistic degradations, allowing geometry-aware learning and evaluation. (2) It covers multiple media, including both underwater and haze/fog, within a unified benchmark. (3) It includes six controlled degradation levels for each scenario for fine-grained performance analysis. (4) It simultaneously provides photometric and geometric GTs without degradation.

We further evaluate two representative existing methods for stereo image restoration under various degradation conditions using the dataset [36] as benchmark. By providing aligned stereo pairs

*Correspondence

†Correspondence

with controllable degradations, M³D-Stereo supports research on geometry-aware restoration, where geometric consistency between stereo views serves as an additional constraint for recovering degraded images through cross-view information fusion [7, 32]. We expect that M³D-Stereo will facilitate future research in stereo image restoration and also support more challenging tasks, such as color-depth joint restoration [21] and stereo matching [34] in adverse environments.

2 Related Work

To put the proposed dataset in context, we classify existing relevant degradation datasets into four main categories: *Monocular Synthetic*, *Monocular Real*, *Stereo Synthetic*, and *Stereo Real*. A detailed summary of the datasets is given in Table 1.

2.1 Synthetic Monocular Degradation Datasets

Such datasets are widely used because they provide precise control over degradation parameters and, in some cases, auxiliary information such as depth. Representative examples, such as SynFog [39], generate degraded images by applying physically inspired models or rendering techniques to clear images to simulate conditions such as low-light or scatter. Although these datasets offer clear advantages in scalability and controllability, they suffer from two fundamental limitations. First, they are restricted to monocular settings and do not provide stereo image pairs, making them unsuitable for geometry-aware learning [32]. Second, synthetic rendering often fails to capture the complex physical processes of real-world environments, such as multiple scatter, wavelength-dependent attenuation, spatially varying illumination, and device noise [29]. As a result, models trained on such datasets often generalize poorly to real scenes. In particular, the inability to faithfully reproduce the combined effects of scatter and absorption in real physical environments leads to a substantial domain gap.

2.2 Real Monocular Degradation Datasets

This category of datasets captures visual degradations in the real physical environments. For example, O-HAZE [3] and Dense-Haze [2] use dedicated haze generation systems to create realistic atmospheric conditions, while datasets such as BeDDE [46], RUIE [20], and UIEB [18] collect natural images in foggy or underwater environments. Although these datasets offer high photometric fidelity, they are fundamentally limited by their monocular nature. They do not provide GTs and stereo correspondences, which restricts their use in geometry-aware tasks [35]. In addition, they often model degradation only as a binary condition, e.g., degraded versus clear, or as a coarse category, and therefore lack the fine-grained and controllable degradation levels needed for more systematic evaluation.

2.3 Synthetic Stereo Degradation Datasets

To evaluate stereo matching in adverse conditions while retaining perfectly dense matching GTs, the dominant strategy is to synthesize degradation effects on top of clear stereo image pairs. Representative examples include HazyKITTI2012 [9, 31], LLHolopix50 [45], LLFlickr2014 [30, 45], and LLKitti2015 [24, 45], which simulate haze/fog or low-light degradations in driving scenes. More recently,

UWStereo rendered a large-scale underwater stereo dataset using Unreal Engine [22]. Although these datasets provide large-scale stereo pairs together with pixel-accurate disparity GTs, synthetic rendering still struggles to reproduce the device noise, non-uniform illumination, and complex medium effects present in real environments. As a result, models trained on such benchmarks often experience substantial performance degradation [42] when deployed in real adverse conditions.

2.4 Real Stereo Degradation Datasets

This category includes a small number of pioneering datasets that capture stereo image pairs in real-world environments. For example, SQUID [4] collected natural underwater stereo images, while DrivingStereo [41] recorded driving scenes under various weather conditions. These datasets provide both physical realism and stereo observations. However, their main limitation lies in the uncontrollable nature of open-world environments, where photometric GTs are not available, and degradation factors such as fog density or water turbidity cannot be precisely adjusted. As a result, they do not provide systematically defined degradation levels, making fine-grained analysis of algorithm robustness under increasing degradation difficult [5]. In fact, achieving strict and progressive degradation levels for the same scene in natural weather is physically infeasible [26].

As discussed above, existing datasets are typically limited to a single degradation scenario and therefore do not reflect the complexity of the cross-domain encountered in real-world deployments [14]. Moreover, there exists a fundamental trade-off between physical realism and controllability [26]: synthetic datasets provide precise control but lack realism, whereas real-world datasets capture authentic degradations but do not offer systematic variations.

In contrast, M³D-Stereo is intended to provide both comprehensiveness and controllability. It fills an important gap in stereo benchmarks for adverse environments and helps bridge underwater and atmospheric vision research within a unified framework. By alleviating the conventional conflict between realism and control, M³D-Stereo integrates multiple media while maintaining strictly controlled progressive degradation levels. In addition, it provides high-quality aligned stereo pairs, photometric GTs, and accurate dense disparity GTs, even under coupled degradation conditions [23]. By overcoming the limitations of existing datasets, it establishes a new benchmark for evaluating stereo restoration and geometry-aware methods under complex real-world degradations.

3 Dataset Construction

This section describes the construction of the M³D-Stereo, including the experimental platform, scene design, degradation generation, and data acquisition pipeline.

3.1 Experimental Setup and Scene Construction

Building on the experience of a previous small-scale study on underwater imaging [21, 33], we redesigned the image acquisition platform to include a high-precision three-axis XYZ translation stage (XG100, Ruibo), two ZED stereo cameras (ZED Mini, Stereolabs), a ring light, and a custom glass tank of size 80 × 80 × 60 cm³. Figure 1(a) shows the underwater stereo acquisition System, which

Table 1: Comparison of imaging degradation datasets (UW: underwater; GT: ground truth).

Category	Dataset	Degradation	Resolution	Syn/Real	Size	Aligned	GT	Task
Synthetic	HazyKITTI2012 [9, 31]	Haze	1242×375	Syn	778	Yes	Yes	Stereo Image Restoration
	HazyKITTI2015 [9, 31]	Haze	1242×375	Syn	800	Yes	Yes	Stereo Image Restoration
	LLHolopix50 [45]	Low-light	1280×720	Syn	1189	Yes	Yes	Stereo Image Restoration
	LLFlickr2014 [30, 45]	Low-light	600×1696	Syn	391	Yes	Yes	Stereo Image Restoration
	LLKitti2015 [24, 45]	Low-light	1242×375	Syn	400	Yes	Yes	Stereo Image Restoration
	UWStereo [22]	UW	1280×720	Syn	29568	Yes	No	Stereo Matching
Real	SQUID [4]	UW scatter	1827×2737	Real	57	Yes	No	Stereo Image Restoration
	DrivingStereo [41]	Fog/Driving	1762×800	Real	500	Yes	No	Stereo Matching
M ³ D-Stereo	UWST subset (Ours)	UW scatter	1920×1080	Real	1536	Yes	Yes	Stereo Image Restoration
	UWLL subset (Ours)	UW low-light	1920×1080	Real	1536	Yes	Yes	Stereo Image Restoration
	HZST subset (Ours)	Haze/Fog	1920×1080	Real	2112	Yes	Yes	Stereo Image Restoration
	HZLL subset (Ours)	Haze low-light	1920×1080	Real	2112	Yes	Yes	Stereo Image Restoration
	Combined (Ours)	4 scenarios	1920×1080	Real	7296	Yes	Yes	Stereo Image Restoration

is used to capture UWST and UWLL images. Figure 1(b) presents the Haze stereo system for acquisition of HZST and HZLL images. The acquisition platform is placed in a closed room so that ambient light can be completely eliminated when room lights are off.

To ensure scene diversity and structural richness, we constructed multiple modular scenes underwater and in air. The underwater scenes contain rocks, corals, aquatic plants, artificial reefs, shipwreck models, and other small objects. These elements were arranged in different combinations to generate diverse geometric structures and occlusion patterns. In the air, we designed miniature scenes that contain vehicles, pedestrians, and trees, to simulate urban and natural environments under adverse weather conditions. Using modular scene components, the platform can be flexibly re-configured, allowing the creation of a large number of scenes with different layouts and visual appearances. For each scene, before applying any degradation, we captured clear GT images using the same camera and pose to ensure pixel-level spatial alignment with the degraded images.

3.2 Stereo Camera Calibration

Due to the significant refractive-index difference between air and water, conventional calibration parameters estimated in the air cannot satisfy the accuracy requirements of underwater data acquisition. To address this issue, we performed a complete recalibration in both atmospheric and underwater environments following the strategy introduced by Li et al. [19]. Specifically, we adopted Zhang’s method [44] to calibrate the two ZED cameras in both clear water and air. Table 2 shows the reprojection errors (L^{rpj} and R^{rpj} for the left and right cameras, respectively) and the Y-offset (dY) after image rectification, the intrinsic and extrinsic parameters are provided in a separate file in the dataset. The calibration results are visually illustrated in Fig. 2.

3.3 Simulations of Physical Degradation

A key feature of M³D-Stereo is the rigorous control of physical degradation. We construct four distinct scenarios, each with six strictly controlled degradation levels from mild to severe (D1–D6).

Table 2: Stereo camera calibration accuracy.

Cam	Medium	L^{rpj} (px)	R^{rpj} (px)	dY (px)
1	Air	0.0337	0.0343	0.1604
	UW	0.0458	0.0427	0.1250
2	Air	0.0387	0.0382	0.3958
	UW	0.0471	0.0544	0.1358

The UWST subset was generated following the 3D TURBID [8, 33] protocol to simulate underwater scatter. The water turbidity was precisely controlled by progressively injecting a prepared milk solution into the tank. Specifically, 19 grams of milk powder (Xiyu Riji Skimmed Milk Powder) were dissolved in 1000 milliliters of water to form the turbid solution. This solution was introduced in six batches to create progressive degradation levels. An initial volume of 250 milliliters was injected for the first level, followed by five additional batches of 100 milliliters each. The cumulative injected volume at the highest degradation level, D6, reaches 750 milliliters. The UWST subset contains 256 image pairs for each degradation level.

The UWLL subset simulates underwater low-light degradation to mimic dark marine environments at different depths. Illumination was precisely controlled by a digital strobe controller (SJ-DPA60W24V, Shijue Factory) together with a ring light source (SJ-R18090-D80, Shijue Factory). The controller employs pulse-width modulation (PWM) dimming at a frequency of 86 kHz and supports 255 discrete brightness levels (0–255 in decimal), where lower values correspond to darker conditions. To ensure strictly progressive and physically grounded degradation, we fixed the PWM values at six levels, i.e., 11, 9, 7, 5, 3, and 1, and measured the corresponding illumination using a lux meter. For each fixed PWM setting, multiple readings were averaged to reduce measurement variability. The resulting illumination levels are 26.7, 20.8, 15.9, 10.5, 5.6, and 3.1 lux, respectively, providing a reproducible quantification of illumination intensity. The UWLL subset also contains 256 image pairs for each degradation level.

The HZST subset simulates haze/fog scatter degradation within a sealed physical space. A professional fogging system (FILMOG

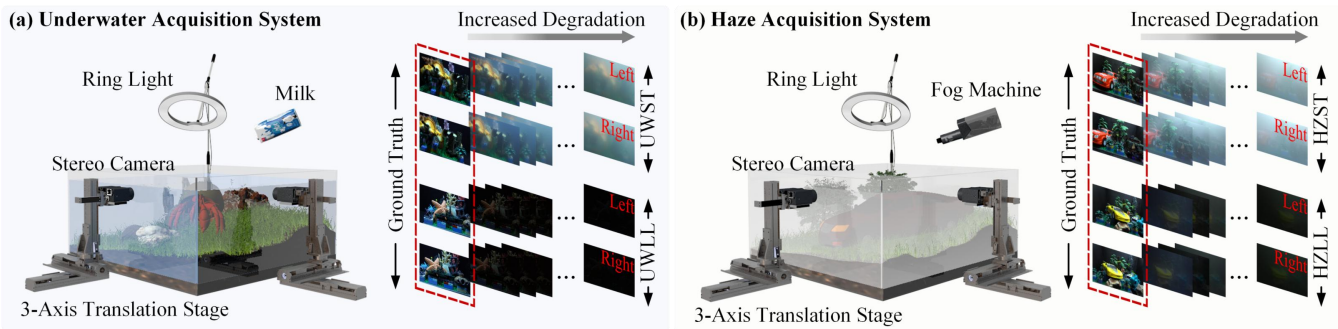


Figure 1: The M³D-Stereo data acquisition platform. (a) Underwater stereo acquisition system: milk is added to the glass tank to simulate underwater scatter at varying concentrations, enabling capturing UWST and UWLL images. (b) Haze stereo acquisition system: a fog machine generates haze scenes of varying density within an enclosed space, enabling the acquisition of HZST and HZLL images. Degradation severity increases along the arrow direction.

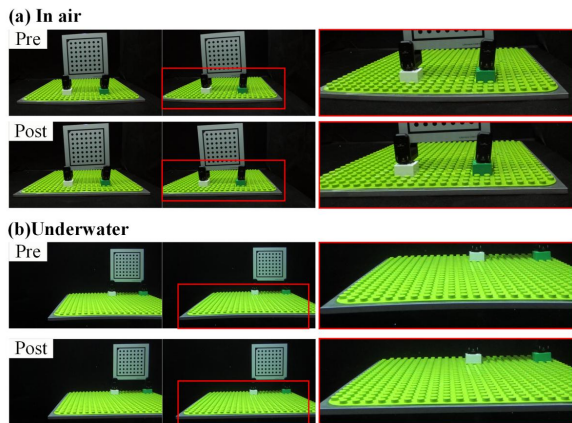


Figure 2: Visualization of stereo calibration accuracy. (a) In air; (b) In clear water. Pre and Post denote the left and right image pairs before and after the calibration, respectively.

ACE portable fog machine, Ulanzi) with precisely controllable spray duration was used to generate haze under strictly progressive concentration levels. The initial spray duration was 10 s, and each subsequent level increases the duration by 5 s. As a result, the cumulative spray duration reaches 35 s at the highest degradation level (D6). By accurately controlling both the release dose and the diffusion time of the physical haze, this procedure creates a realistic fog scatter environment with approximately uniform distribution and well-defined progressive degradation. The HZST subset contains 352 image pairs for each degradation level.

The HZLL subset simulates the coupled degradation of haze/fog and low-light to reproduce highly challenging adverse conditions at night. Specifically, it combines selected levels from the two single-degradation settings. Haze levels D2, D4, and D6 were paired with low-light levels D1 and D3, resulting in six coupled degradation levels. Consequently, the composite levels D1–D6 correspond to: haze D2 + low-light D1, haze D2 + low-light D3, haze D4 + low-light D1, haze D4 + low-light D3, haze D6 + low-light D1 and haze D6 + low-light D3. This physically coupled design better reflects the nonlinear interaction between scatter and weak illumination and significantly increases the difficulty as well as the evaluation value

of stereo image restoration. The HZLL subset also contains 352 image pairs for each degradation level.

To obtain high-quality GT stereo pairs that are pixel-wise aligned with observations across all degradation levels, we adopted a strictly controlled static-locking acquisition protocol. Both the stereo camera and all miniature objects in the scene were rigidly fixed to eliminate micro-motion. Clear stereo GT pairs were first captured under clean-medium and room illumination conditions, and these images serve as the reference for all subsequent acquisitions. The degradation media, such as milk or haze, were then gradually introduced, or the light level was progressively reduced. At each stable degradation level from D1 to D6, stereo image pairs were captured while the scene layout was kept unchanged. This protocol physically guarantees spatial consistency between the degraded observations and their corresponding GTs, thereby providing a reliable basis for stereo restoration and quantitative evaluation.

Table 3 summarizes the degradation conditions and the number of image pairs in each subcategory. It should be noted that UWST and UWLL have the the same GTs of 256 pairs, and HZST and HZLL share the same GTs of 352 pairs. And Fig. 3 illustrates one example image for each of the degradation cases and its clear GT.

Table 3: Summary of M³D-Stereo. Each level specifies the physical control parameter and the stereo image pairs.

Level	UWST		UWLL		HZST		HZLL		
	Milk(ml)	Pairs	Lux	Pairs	Fog(s)	Pairs	Fog(s)	Lux	Pairs
GT	0	(256)	173.7	256	0	(352)	0	141.3	352
D1	250	256	26.7	256	10	352	15	26.7	352
D2	350	256	20.8	256	15	352	15	15.9	352
D3	450	256	15.9	256	20	352	25	26.7	352
D4	550	256	10.5	256	25	352	25	15.9	352
D5	650	256	5.6	256	30	352	35	26.7	352
D6	750	256	3.1	256	35	352	35	15.9	352
Total	—	1536	—	1792	—	2112	—	—	2464

4 Experimental Evaluation

Experimental validation consists of two tasks to evaluate the performance of image restoration methods on the dataset. Under a

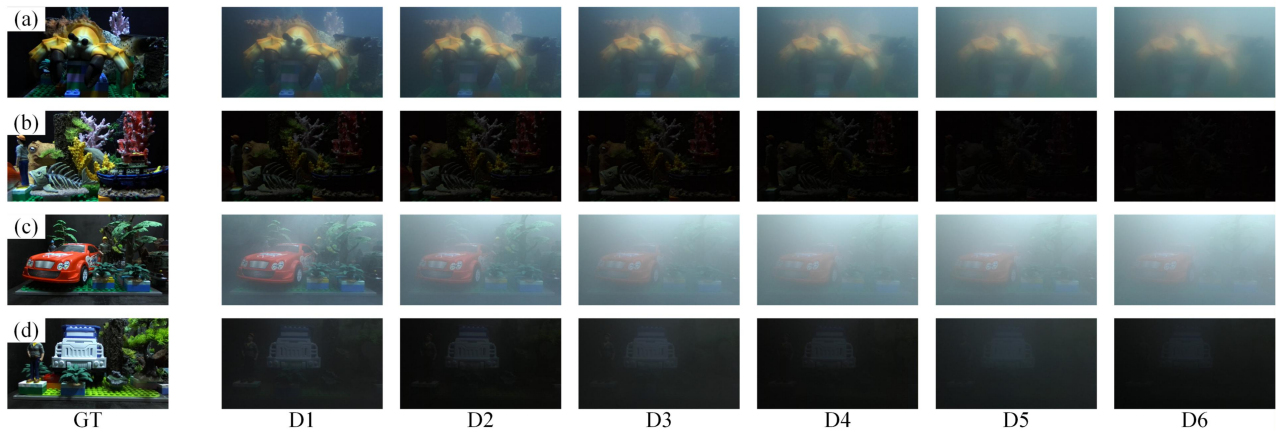


Figure 3: Sample images from the M³D-Stereo dataset at degradation levels D1–D6. The leftmost column shows the clean GT. All displayed samples correspond to the left view only. (a) Underwater scatter (UWST). (b) Underwater low-light (UWLL). (c) Haze scatter (HZST). (d) Haze low-light (HZLL). Degradation severity increases from D1 to D6.

unified protocol, two representative stereo restoration methods, EPRRNet [43] and PSIDNet [31], were evaluated. Experiments were conducted on all four degradation scenarios: UWST, UWLL, HZST, and HZLL. All experiments used the dataset with a consistent training/testing split. To ensure a fair comparison, both methods were trained and tested in identical settings. Performance is evaluated using full-reference image-quality metrics, PSNR and SSIM [13].

4.1 Single-Level Degradation

This task evaluates the restoration performance under different degradation levels. For each scenario, we selected three representative levels with clearly distinct intensities, namely D2, D4, and D6. The models were trained and tested independently on each level. The results are shown in Table 4 and Fig. 4. A consistent trend is observed across all scenarios: as the degradation level increases from D2 to D6, both PSNR and SSIM decrease. This indicates that a stronger degradation causes more severe information loss and makes image restoration increasingly difficult. Similar trends have also been reported in previous studies on low-light enhancement [10, 17] and dehazing [6, 12, 18], where performance degradation is closely associated with reduced signal quality.

Table 4: Restoration results for single-level degradation.

Scen	Model	D2		D4		D6	
		PSNR↑	SSIM↑	PSNR↑	SSIM↑	PSNR↑	SSIM↑
UWST	EPRRNet	18.46	0.6316	16.17	0.4989	13.92	0.4059
	PSIDNet	21.47	0.7740	19.79	0.6804	17.28	0.5694
UWLL	EPRRNet	24.26	0.8266	23.02	0.8112	19.46	0.7076
	PSIDNet	25.06	0.8614	25.08	0.8499	23.20	0.7835
HZST	EPRRNet	21.93	0.7408	17.30	0.5283	16.17	0.4428
	PSIDNet	24.81	0.8381	21.29	0.7307	19.71	0.6556
HZLL	EPRRNet	18.80	0.5803	16.405	0.4310	15.795	0.4059
	PSIDNet	20.835	0.7101	18.015	0.5820	14.575	0.4977

Across all evaluated settings, PSIDNet consistently achieves higher PSNR and SSIM values than EPRRNet. The performance

Table 5: Image restoration results for mixed-level degradation. Six levels (D1–D6) were mixed for training and testing.

Scen	Model	Left view			Right view		
		PSNR↑	SSIM↑	ΔE ↓	PSNR↑	SSIM↑	ΔE ↓
UWST	EPRRNet	18.60	0.6194	11.22	19.17	0.6314	11.03
	PSIDNet	21.04	0.7348	8.20	21.07	0.7347	8.27
UWLL	EPRRNet	20.61	0.6795	8.77	20.86	0.6790	8.50
	PSIDNet	23.23	0.7795	6.36	23.63	0.7814	6.18
HZST	EPRRNet	20.48	0.7380	9.33	20.88	0.7483	9.04
	PSIDNet	24.37	0.8226	6.13	24.08	0.8223	6.52
HZLL	EPRRNet	17.48	0.5066	13.05	17.78	0.5051	12.95
	PSIDNet	18.48	0.6269	10.55	18.94	0.6261	10.28

gap becomes more pronounced with increased severity of degradation. For example, under HZST at D4 and D6, PSIDNet maintains more stable structural similarity, indicating stronger robustness to moderate and severe scatter effects. A similar trend is observed for UWST, suggesting that PSIDNet preserves more image details under severe turbidity. These results show that stereo image restoration methods can maintain relatively stable performance at different degradation levels, while different network architectures exhibit noticeably different robustness under challenging conditions.

4.2 Mixed-level Degradation

This task evaluates a model’s ability to handle mixed degradation levels using a single set of weights. For each subset, we combined all training samples from D1 to D6 to train one model. During testing, performance was evaluated separately at each degradation level and the final results are reported as average of all levels. In addition to PSNR and SSIM, we also use ΔE [11] to evaluate color fidelity, where a lower ΔE indicates better performance.

4.3 Stereo Matching Evaluation

To show the benefit of stereo restoration for downstream stereo matching, we fed degraded images, PSIDNet restored results, and

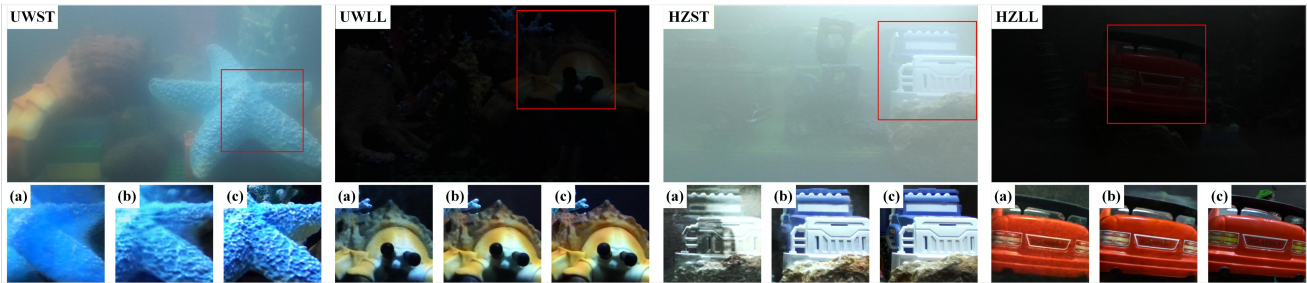


Figure 4: Restoration examples on the M³D-Stereo dataset across four degradation scenarios. From left to right: UWST, UWLL, HZST, and HZLL. The top row shows the full degraded images, and the bottom row shows zoomed-in comparisons of the red-box regions from: (a) EPRRNet restoration; (b) PSIDNet restoration; (c) clean GT.

clean GTs into a pre-trained FoundationStereo model [38] for depth estimation. As illustrated in Fig. 5, the depth map obtained by stereo matching on the degraded images exhibits severely distorted structures, with the background almost indistinguishable. In the depth map from restored images by PSIDNet, object contours become identifiable and depth layering is partially recovered. This comparison demonstrates that stereo image restoration can significantly improve the reliability of stereo matching under severe degradation.

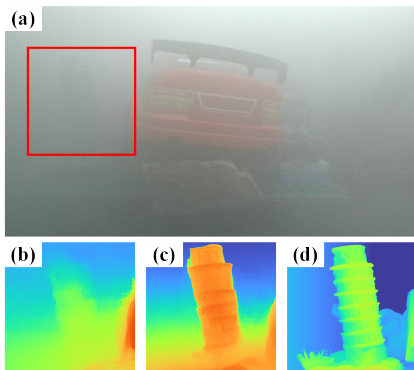


Figure 5: Impact of image restoration on stereo matching by pretrained FoundationStereo. (a) Degraded input (left view). (b) Depth map from degraded images. (c) Depth map from PSIDNet restored images. (d) Depth map from GTs.

5 Access and Licensing

The dataset will be made public on Huggingface <https://huggingface.co/datasets/M3D-Stereo/M3D-Stereo>, under LGPLv3 license.

6 Conclusion and Limitations

This paper introduces M³D-Stereo, a public dataset of multiple-medium stereo image restoration. It unifies underwater and atmospheric environments within a single framework and covers four degradation scenarios: UWST, UWLL, HZST and HZLL. Each scenario is further divided into six progressive degradation levels, enabling systematic evaluation under increasing degradation severity. It was acquired using a laboratory setup that balances physical realism with precise control over degradation factors. The dataset provides aligned stereo image pairs together with the corresponding GTs, enabling better evaluations of restoration performance.

M³D-Stereo was validated with two stereo restoration methods for single-level and mixed-level degradation settings as a benchmark. Results show that restoration performance consistently declines as degradation becomes stronger, while training on mixed degradation levels improves model robustness.

Despite the advantages, M³D-Stereo has some limitations. First, it was acquired in a controlled environment with miniaturized objects and does not fully capture the scale of natural scenes. Second, although it covers multiple scenarios, its diversity remains limited compared to the real environment. Third, the current haze/fog and low-light coupled degradation is still limited in combinations. Future directions include extending the dataset to more complex environments, incorporating additional scenarios, such as rain and dust, and exploring its use in geometry-aware tasks such as stereo matching and color-depth joint restoration. We expect M³D-Stereo to serve as a useful benchmark for research on stereo image restoration and stereo matching under complex degradations.

Acknowledgments

National Key R&D Program of China (2024YFB4710600), LingChuang Research Project of China National Nuclear Corporation (CNNC-LCKY-2024-072), Shenzhen Science and Technology Innovation Commission (JCYJ20240813141402003) and Shenzhen Talent Startup Funds (827-000954).

References

- [1] Derya Akkaynak and Tali Treibitz. 2019. Sea-Thru: A Method for Removing Water From Underwater Images. *2019 IEEE/CVF Conference on Computer Vision and Pattern Recognition (CVPR)* (2019), 1682–1691.
- [2] Codruta Ormiana Ancuti, Cosmin Ancuți, Mateu Sbert, and Radu Timofte. 2019. Dense-Haze: A Benchmark for Image Dehazing with Dense-Haze and Haze-Free Images. *2019 IEEE International Conference on Image Processing (ICIP)* (2019), 1014–1018.
- [3] Codruta Ormiana Ancuti, Cosmin Ancuți, Radu Timofte, and Christophe De Vleeschouwer. 2018. O-HAZE: A Dehazing Benchmark with Real Hazy and Haze-Free Outdoor Images. *2018 IEEE/CVF Conference on Computer Vision and Pattern Recognition Workshops (CVPRW)* (2018), 867–8678.
- [4] Dana Berman, Deborah Levy, Shai Avidan, and Tali Treibitz. 2018. Underwater Single Image Color Restoration Using Haze-Lines and a New Quantitative Dataset. *IEEE Transactions on Pattern Analysis and Machine Intelligence* 43 (2018), 2822–2837.
- [5] Mario Bijelic, Tobias Gruber, Fahim Mannan, Florian Kraus, Werner Ritter, Klaus C. J. Dietmayer, and Felix Heide. 2019. Seeing Through Fog Without Seeing Fog: Deep Multimodal Sensor Fusion in Unseen Adverse Weather. *2020 IEEE/CVF Conference on Computer Vision and Pattern Recognition (CVPR)* (2019), 11679–11689.

- [6] Bolun Cai, Xiangmin Xu, Kui Jia, Chunmei Qing, and Dacheng Tao. 2016. DehazeNet: An End-to-End System for Single Image Haze Removal. *IEEE Transactions on Image Processing* 25 (2016), 5187–5198.
- [7] Xiaojie Chu, Liangyu Chen, and Wenqing Yu. 2022. NAFSSR: Stereo Image Super-Resolution Using NAFNet. *2022 IEEE/CVF Conference on Computer Vision and Pattern Recognition Workshops (CVPRW)* (2022), 1238–1247.
- [8] Amanda C. Duarte, Felipe Codevilla, Joel De O Gaya, and Silvia S. C. Botelho. 2016. A dataset to evaluate underwater image restoration methods. *OCEANS 2016 - Shanghai* (2016), 1–6.
- [9] Andreas Geiger, Philip Lenz, Christoph Stiller, and Raquel Urtasun. 2013. Vision meets robotics: The KITTI dataset. *The International Journal of Robotics Research* 32 (2013), 1231 – 1237.
- [10] Chunle Guo, Chongyi Li, Jichang Guo, Chen Change Loy, Junhui Hou, Sam Tak Wu Kwong, and Runmin Cong. 2020. Zero-Reference Deep Curve Estimation for Low-Light Image Enhancement. *2020 IEEE/CVF Conference on Computer Vision and Pattern Recognition (CVPR)* (2020), 1777–1786.
- [11] Martin Habekost. 2013. Which color differencing equation should be used? *International Circular of Graphic Education and Research* 6 (2013), 20–33.
- [12] Kaiming He, Jian Sun, and Xiaoou Tang. 2009. Single image haze removal using dark channel prior. *2009 IEEE Conference on Computer Vision and Pattern Recognition* (2009), 1956–1963.
- [13] Alain Horé and Djemel Ziou. 2010. Image Quality Metrics: PSNR vs. SSIM. In *2010 20th International Conference on Pattern Recognition*. 2366–2369.
- [14] Junjun Jiang, Zengyuan Zuo, Gang Wu, Kui Jiang, and Xianming Liu. 2024. A Survey on All-in-One Image Restoration: Taxonomy, Evaluation and Future Trends. *IEEE Transactions on Pattern Analysis and Machine Intelligence* 47 (2024), 11892–11911.
- [15] Alex Kendall, Hayk Martirosyan, Saumitro Dasgupta, and Peter Henry. 2017. End-to-End Learning of Geometry and Context for Deep Stereo Regression. *2017 IEEE International Conference on Computer Vision (ICCV)* (2017), 66–75.
- [16] Chongyi Li, Saeed Anwar, Junhui Hou, Runmin Cong, Chunle Guo, and Wenqi Ren. 2021. Underwater Image Enhancement via Medium Transmission-Guided Multi-Color Space Embedding. *IEEE Transactions on Image Processing* 30 (2021), 4985–5000.
- [17] Chongyi Li, Chunle Guo, Linghao Han, Jun Jiang, Ming-Ming Cheng, Jinwei Gu, and Chen Change Loy. 2022. Low-Light Image and Video Enhancement Using Deep Learning: A Survey. *IEEE Transactions on Pattern Analysis and Machine Intelligence* 44, 12 (2022), 9396–9416.
- [18] Chongyi Li, Chunle Guo, Wenqi Ren, Runmin Cong, Junhui Hou, Sam Tak Wu Kwong, and Dacheng Tao. 2019. An Underwater Image Enhancement Benchmark Dataset and Beyond. *IEEE Transactions on Image Processing* 29 (2019), 4376–4389.
- [19] Zeping Li, Yixin Chen, Hao Fan, and Junyu Dong. 2023. Evaluating The Effect of Refraction on Underwater Stereo Vision. *2023 IEEE Smart World Congress (SWC)* (2023), 1–6.
- [20] Risheng Liu, Xin Fan, Ming Zhu, Minjun Hou, and Zhongxuan Luo. 2019. Real-World Underwater Enhancement: Challenges, Benchmarks, and Solutions Under Natural Light. *IEEE Transactions on Circuits and Systems for Video Technology* 30 (2019), 4861–4875.
- [21] Dajiang Lu, Qicong Wang, Xiaopin Zhong, and Yibin Tian. 2025. Multi-task Learning for Simultaneous Underwater Color Image Restoration and Monocular Depth Estimation. In *International Conference on Intelligent Computing*. Springer, 52–66.
- [22] Qingxuan Lv, Junyu Dong, Yuezun Li, Sheng Chen, Hui Yu, Shu Zhang, and Wenhan Wang. 2024. UWStereo: A Large Synthetic Dataset for Underwater Stereo Matching. *IEEE Transactions on Circuits and Systems for Video Technology* 35 (2024), 11216–11228.
- [23] Nikolaus Mayer, Eddy Ilg, Philip Häusser, Philipp Fischer, Daniel Cremers, Alexey Dosovitskiy, and Thomas Brox. 2015. A Large Dataset to Train Convolutional Networks for Disparity, Optical Flow, and Scene Flow Estimation. *2016 IEEE Conference on Computer Vision and Pattern Recognition (CVPR)* (2015), 4040–4048.
- [24] Moritz Menze and Andreas Geiger. 2015. Object scene flow for autonomous vehicles. *2015 IEEE Conference on Computer Vision and Pattern Recognition (CVPR)* (2015), 3061–3070.
- [25] Wenqi Ren, Sibao Liu, Hua Zhang, Jin shan Pan, Xiaochun Cao, and Ming-Hsuan Yang. 2016. Single Image Dehazing via Multi-scale Convolutional Neural Networks. In *European Conference on Computer Vision*.
- [26] Christos Sakaridis, Dengxin Dai, and Luc Van Gool. 2017. Semantic Foggy Scene Understanding with Synthetic Data. *International Journal of Computer Vision* 126 (2017), 973 – 992.
- [27] Daniel Scharstein, Heiko Hirschmüller, York Kitajima, Greg Krathwohl, Nera Nesić, Xi Wang, and Porter Westling. 2014. High-Resolution Stereo Datasets with Subpixel-Accurate Ground Truth. In *German Conference on Pattern Recognition*.
- [28] Daniel Scharstein and Richard Szeliski. 2001. A Taxonomy and Evaluation of Dense Two-Frame Stereo Correspondence Algorithms. *International Journal of Computer Vision* 47 (2001), 7–42.
- [29] Yuanjie Shao, Lerenhan Li, Wenqi Ren, Changxin Gao, and Nong Sang. 2020. Domain Adaptation for Image Dehazing. *2020 IEEE/CVF Conference on Computer Vision and Pattern Recognition (CVPR)* (2020), 2805–2814.
- [30] Bart Thomee, David A. Shamma, Gerald Friedland, Benjamin Elizalde, Karl S. Ni, Douglas N. Poland, Damian Borth, and Li-Jia Li. 2015. YFCC100M. *Commun. ACM* 59 (2015), 64 – 73.
- [31] Junhu Wang, Yanyan Wei, Zhao Zhang, Jicong Fan, Yang Zhao, Yi Yang, and Meng Wang. 2024. Progressive Stereo Image Dehazing Network via Cross-View Region Interaction. *IEEE Transactions on Multimedia* 26 (2024), 7490–7502.
- [32] Longguang Wang, Yingqian Wang, Zhengfa Liang, Zaiping Lin, Jungang Yang, Wei An, and Yulan Guo. 2019. Learning Parallax Attention for Stereo Image Super-Resolution. *2019 IEEE/CVF Conference on Computer Vision and Pattern Recognition (CVPR)* (2019), 12242–12251.
- [33] Qicong Wang, Xiaopin Zhong, Dajiang Lu, and Yibin Tian. 2025. ITW-DehazeFormer: Imaging through Turbid Water Using Improved DehazeFormer. In *ICASSP 2025-2025 IEEE International Conference on Acoustics, Speech and Signal Processing (ICASSP)*. IEEE, 1–5.
- [34] Yun Wang, Junjie Hu, Junhui Hou, Chenghao Zhang, Renwei Yang, and Dapeng Wu. 2025. RoSe: Robust Self-supervised Stereo Matching under Adverse Weather Conditions. *ArXiv abs/2509.19165* (2025).
- [35] Yuran Wang, Yingping Liang, Yutao Hu, and Ying Fu. 2025. RobuStereo: Robust Zero-Shot Stereo Matching under Adverse Weather. *ArXiv abs/2507.01653* (2025).
- [36] Yingqian Wang, Longguang Wang, Jungang Yang, Wei An, and Yulan Guo. 2019. Flickr1024: A Large-Scale Dataset for Stereo Image Super-Resolution. *2019 IEEE/CVF International Conference on Computer Vision Workshop (ICCVW)* (2019), 3852–3857.
- [37] Chen Wei, Wenjing Wang, Wenhan Yang, and Jiaying Liu. 2018. Deep Retinex Decomposition for Low-Light Enhancement. *ArXiv abs/1808.04560* (2018).
- [38] Bowen Wen, Matthew Trepte, J. Arribido, Jan Kautz, Orazio Gallo, and Stanley T. Birchfield. 2025. FoundationStereo: Zero-Shot Stereo Matching. *2025 IEEE/CVF Conference on Computer Vision and Pattern Recognition (CVPR)* (2025), 5249–5260.
- [39] Yiming Xie, Henglu Wei, Zhenyi Liu, Xiaoyu Wang, and Xiangyang Ji. 2024. SynFog: A Photorealistic Synthetic Fog Dataset Based on End-to-End Imaging Simulation for Advancing Real-World Defogging in Autonomous Driving. *2024 IEEE/CVF Conference on Computer Vision and Pattern Recognition (CVPR)* (2024), 21763–21772.
- [40] Shuaizheng Yan, Xingyu Chen, Zhengxing Wu, Min Tan, and Junzhi Yu. 2023. HybrUR: A Hybrid Physical-Neural Solution for Unsupervised Underwater Image Restoration. *IEEE Transactions on Image Processing* 32 (2023), 5004–5016.
- [41] Guorun Yang, Xiao Song, Chaoqin Huang, Zhidong Deng, Jianping Shi, and Bolei Zhou. 2019. DrivingStereo: A Large-Scale Dataset for Stereo Matching in Autonomous Driving Scenarios. *2019 IEEE/CVF Conference on Computer Vision and Pattern Recognition (CVPR)* (2019), 899–908.
- [42] Feihu Zhang, Xiaojuan Qi, Ruigang Yang, Victor Adrian Prisacariu, Benjamin W. Wah, and Philip H. S. Torr. 2019. Domain-invariant Stereo Matching Networks. *ArXiv abs/1911.13287* (2019).
- [43] Kaihao Zhang, Wenhan Luo, Wenqi Ren, Jingwen Wang, Fang Zhao, Lin Ma, and Hongdong Li. 2020. Beyond Monocular Deraining: Stereo Image Deraining via Semantic Understanding. In *European Conference on Computer Vision*.
- [44] Zhengyou Zhang. 2000. A Flexible New Technique for Camera Calibration. *IEEE Trans. Pattern Anal. Mach. Intell.* 22 (2000), 1330–1334.
- [45] Minghua Zhao, Xiangdong Qin, Shuangli Du, Xuefei Bai, Jiahao Lyu, and Yiguang Liu. 2024. Low-light Stereo Image Enhancement and De-noising in the Low-frequency Information Enhanced Image Space. *Expert Syst. Appl.* 265 (2024), 125803.
- [46] Shiyu Zhao, Lin Zhang, Shuaiyi Huang, Ying Shen, and Shengjie Zhao. 2020. Dehazing Evaluation: Real-World Benchmark Datasets, Criteria, and Baselines. *IEEE Transactions on Image Processing* 29 (2020), 6947–6962.